Developmental Cell *10*, 223–232, February, 2006 ©2006 Elsevier Inc. DOI 10.1016/j.devcel.2005.12.012

The Physiological Function of von Willebrand's Factor Depends on Its Tubular Storage in Endothelial Weibel-Palade Bodies

Grégoire Michaux,[1] Kate B. Abbitt,[2] Lucy M. Collinson,[1] Sandra L. Haberichter,[3,4] Keith E. Norman,[2] and Daniel F. Cutler[1,*]

[1] MRC Laboratory for Molecular Cell Biology
Cell Biology Unit and Department of Biochemistry
University College London
Gower Street
London WC1E 6BT
United Kingdom

[2] Cardiovascular Research Unit
University of Sheffield Clinical Sciences Centre
Northern General Hospital
Sheffield S5 7AU
United Kingdom

[3] Department of Pediatrics
Medical College of Wisconsin
Milwaukee, Wisconsin 53226

[4] Children's Research Institute
Children's Hospital of Wisconsin
Milwaukee, Wisconsin 53201

Summary

Weibel-Palade bodies are the 1–5 μm long rod-shaped storage organelles of endothelial cells. We have investigated the determinants and functional significance of this shape. We find that the folding of the hemostatic protein von Willebrand's factor (VWF) into tubules underpins the rod-like shape of Weibel-Palade bodies. Further, while the propeptide and the N-terminal domains of mature VWF are sufficient to form tubules, their maintenance relies on a pH-dependent interaction between the two. We show that the tubular conformation of VWF is essential for a rapid unfurling of 100 μm long, platelet-catching VWF filaments when exposed to neutral pH after exocytosis in cell culture and in living blood vessels. If tubules are disassembled prior to exocytosis, then short or tangled filaments are released and platelet recruitment is reduced. Thus, a 100-fold compaction of VWF into tubules determines the unique shape of Weibel-Palade bodies and is critical to this protein's hemostatic function.

Introduction

Many proteins are stored within the secretory granules of cells, to be released only upon stimulation-dependent exocytosis. Despite the very different functions carried out by these hormones, zymogens, and other secretory proteins, their storage organelles are generally variants on a sphere, presumably reflecting the high storage capacity of this shape. However, within the granules, the content exhibits a wide variety of structures—from amorphous to tubular to crystalline. Does the storage format of these proteins simply reflect the effects of concentrating the content as much as possible to maximize storage, or is there any postexocytic functional significance to these structures? To address this general question, we have examined the granules of endothelial cells that contain a tubular cargo.

The hemostatic protein von Willebrand's factor (VWF) is stored within the uniquely rod-shaped Weibel-Palade bodies (WPBs) (Wagner et al., 1982; Weibel and Palade, 1964) in endothelial cells. After secretagogue stimulation, WPBs undergo exocytosis, releasing ultralong (100 μm in average) VWF filaments that capture platelets along their lengths (Andre et al., 2000; Dong et al., 2002). Subsequent activation and aggregation of platelets cause the formation of a hemostatic plug (Ruggeri, 2003b). Failure to secrete ultralong VWF filaments upon WPB exocytosis, as in von Willebrand's disease, in which VWF is mutated, leads to excessive bleeding (Ruggeri, 2003a; Sadler, 2005).

VWF filament formation in endothelial cells is a complex process (Michaux and Cutler, 2004; Sadler, 1998; van Mourik et al., 2002). First, in the ER, disulphide bonds form between C-terminal domains, causing dimerization. Second, in the Golgi, disulphide bonds are formed between the N-terminal D′-D3 domains of the dimers, leading to multimerization of mature VWF. Before or during N-terminal bonding, Furin-dependent cleavage of the 741 amino acid propeptide occurs (Wise et al., 1990). This process ultimately generates a very large multimer composed only of mature VWF; the propeptide acts as a cofactor supporting N-terminal disulphide bond formation and remains noncovalently associated with mature VWF in a 1:1 stoichiometry in WPBs (Ewenstein et al., 1987; Wagner et al., 1987). The VWF multimers then adopt a tubular conformation and are stored in rigid, rod-like WPBs of 1–5 μm (Wagner et al., 1982; Weibel and Palade, 1964). While the propeptide is rapidly dispersed in the bloodstream at exocytosis (Hannah et al., 2005), the multimeric filaments unfurl rapidly, within 15 s of stimulation in mice (Andre et al., 2000). Organizing them into a comparatively small organelle, yet preventing their entanglement inside WPBs prior to secretion and upon unfurling, must require sophisticated packing. We hypothesized that tubulation might be required for efficient unfurling and the subsequent hemostatic function of VWF.

We first established a strict correlation between WPB elongation and VWF tubulation. We show that it involves a pH-dependent interaction between the propeptide and the first three domains of the mature protein and does not require multimerization, confirming that tubulation is independent of multimerization (Wagner et al., 1991). Second, we demonstrate that the compact storage of the filaments requires an acidic pH and an interaction with the propeptide. Finally, we show that both tubular storage and multimerization are necessary for the rapid unfurling of the long VWF filaments from stimulated endothelial cells in culture and in laser-injured cremaster venules in mice, as tested by their ability to recruit platelets. We conclude that the unusual elongated shape of WPBs is dictated by VWF folding into the tubules that are necessary for correct and rapid unfurling of the

*Correspondence: d.cutler@ucl.ac.uk

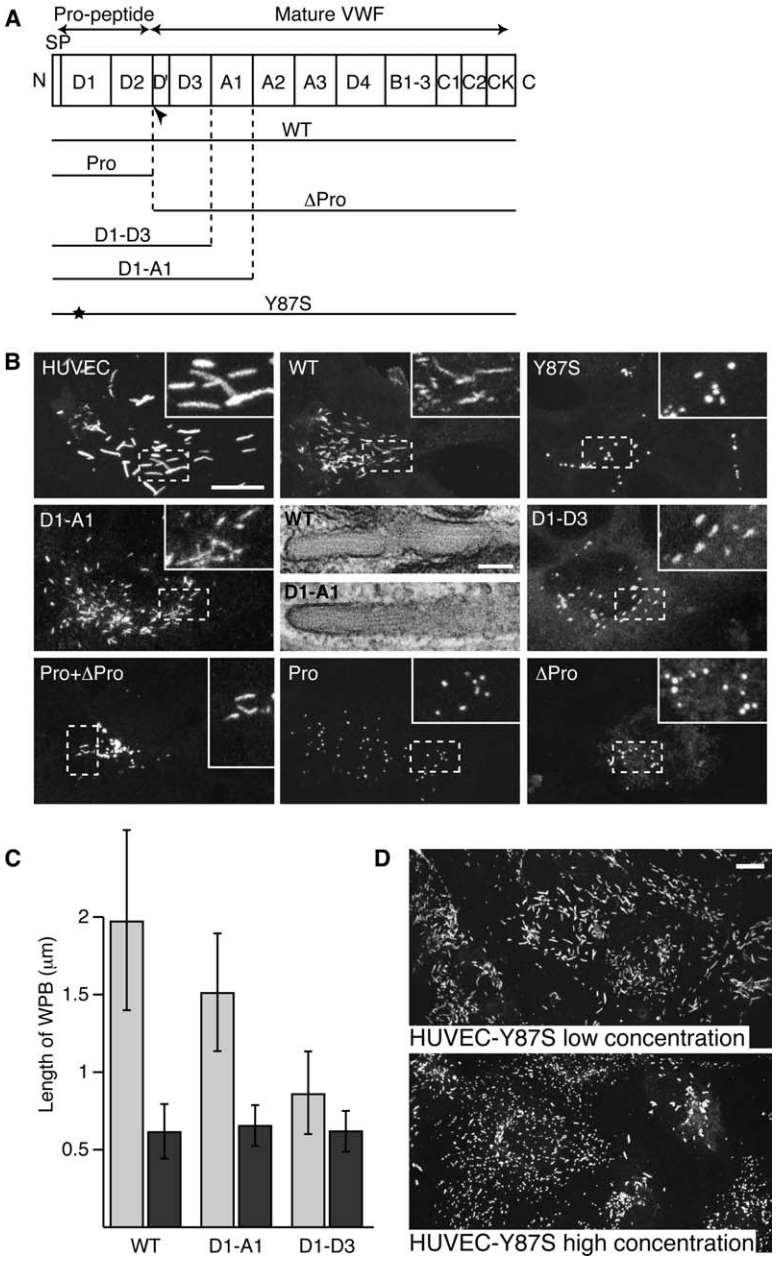

Figure 1. The D1-A1 Domains of VWF Are Both Necessary and Sufficient for VWF Tubulation and WPB Elongation

(A) VWF is drawn roughly to scale, showing its domain structure; the constructs used are shown underneath. SP, signal peptide; Pro, propeptide; Δpro, mature VWF. The star within Y87S indicates the location of this tyrosine-to-serine mutation. The furin cleavage site is indicated by an arrowhead.

(B) Light and electron microscopic analyses of the VWF-positive structures produced by the various constructs. Apart from the upper-left panel (HUVECs), HEK293 cells were nucleofected with the indicated VWF construct; 2 days later, they were fixed and stained for mature VWF or the propeptide and were analyzed by light microscopy. In the two central panels, cells were analyzed by electron microscopy. The insets are enlargements of the regions boxed with a dashed line. Elongated WPBs can be observed with WT, D1-A1, D1-D3, and Pro+Δpro constructs, but only round, VWF-positive structures are observed after Pro, Δpro, or Y87S constructs. Scale bars represent 10 μm (100 nm in electron micrographs).

(C) The size of elongated (light gray) and round (dark gray) WPBs was measured after expression of WT-VWF, D1-A1, and D1-D3. Bars represent mean ± standard deviation ($n \geq 100$ WPBs for each bar).

(D) HUVECs were nucleofected with Y87S at low or high concentration, left for 24 hr, and stained with anti-VWF. Shorter WPBs can be observed in the lower panel. The scale bar represents 10 μm.

ultralong VWF filaments, and therefore that the storage format of granule cargo does indeed matter.

Results

The D1-A1 Domains Are Essential to VWF Tubulation and WPB Elongation

In straight WPBs, the VWF tubules generally run from one end of the organelle to the other, strongly suggesting that WPB elongation is driven by the presence of internal VWF tubules (Figure S1; see the Supplemental Data available with this article online). Having previously recapitulated the formation of functional WPBs in HEK293 cells (Michaux et al., 2003), we used this system to determine the VWF domain(s) responsible for WPB elongation. We expressed several VWF deletions and a human mutant VWF that causes severe von Willebrand's disease (Rosenberg et al., 2002) in HEK293 cells (Figures 1A and 1B).

Analysis of deletions revealed that expression of either the propeptide (D1 and D2 domains) or mature VWF (D′ to CK domains) under identical conditions triggers the formation of round, VWF-positive structures alone. Coexpression of both constructs in *trans* led to the formation of many elongated WPBs, indicating that both are necessary for WPB elongation. After expressed VWF was reduced to the D1-D3 domains, most WPBs observed were round; however, a few were slightly elongated (note that the picture was obtained with a c-*myc*-tagged D1-D3, but that slightly elongated WPBs were also seen after expression of an untagged D1-D3 construct or a GFP-tagged D1-D3). In contrast, almost all WPBs were elongated after expression of a truncated VWF containing D1-A1 domains. Measuring the length of elongated

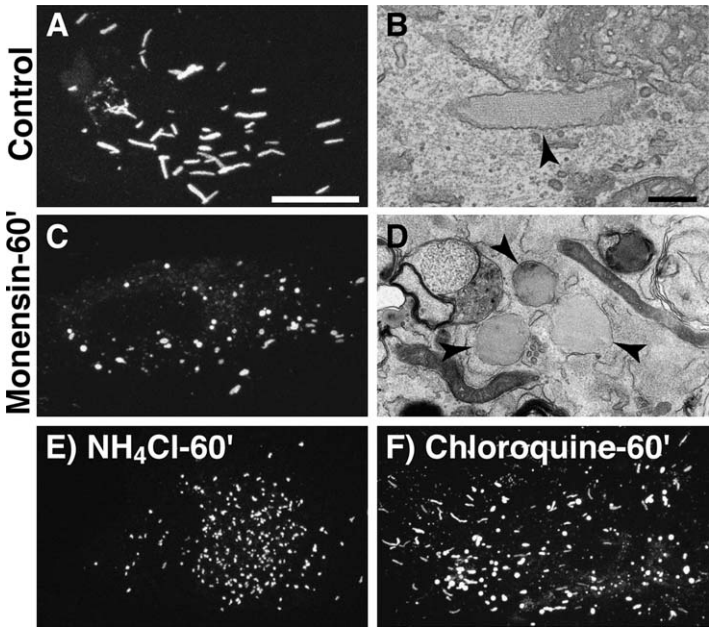

Figure 2. VWF Tubulation and WPB Elongation Are Dependent on an Acidic pH

(A–F) HUVECs were stained for VWF or observed by electron microscopy. (C and D) Monensin, (E) NH_4Cl, or (F) chloroquine were applied for 60 min and altered the elongated shape of WPBs from HUVECs. Arrowheads (B–D) point to WPBs; note that in (D) the tubular organization of VWF has been disrupted by monensin, and that WPBs become spherical. Scale bars represent 10 μm (100 nm in [B] and [D]).

WPBs confirmed that D1-A1 and WT-VWF expression triggered the formation of WPBs significantly longer than those formed after D1-D3 expression (Figure 1C), while the round WPBs seen in varying numbers after expression of all constructs have similar smaller sizes.

To confirm that genuine VWF tubules can be made from the N-terminal half of VWF alone, the ultrastructure of WPBs after D1-A1 expression was examined by EM and was found to be indistinguishable from that found after WT-VWF expression (Figure 1B). To further test the role of the propeptide in VWF tubulation, we also expressed the Y87S variant in both HEK293 cells (Figure 1B) and in human umbilical vein endothelial cells (HUVECs) (Figure 1D). Expression of Y87S led to the formation of round WPBs in HEK293 cells. Transfecting 625 ng per 3.5 cm dish of this construct in HUVECs had no effect on WPB formation or length, but when 25 μg was transfected, the WPBs were much shorter. This difference clearly indicates that the mutant propeptide can have a dominant effect on WPB shape, probably by disrupting the VWF tubules.

We conclude that both the propeptide and D′-D3-A1 domains of mature VWF are required to store VWF as tubules, and that these correlate with WPB elongation.

Maintenance of VWF Tubulation Depends on the Intraorganelle Environment and Is Indeed Responsible for WPB Elongation

WPBs form at the trans-Golgi network (TGN), at which point the pH falls, suggesting that an acidic pH might be needed for tubule formation and thus WPB shape. To test this hypothesis, we incubated HUVECs in the presence of monensin (Figures 2C and 2D), NH_4Cl (Figure 2E), or chloroquine (Figure 2F), all of which neutralize the pH of acidic organelles. These treatments caused most WPBs to become round within 1 hr (Figure 2), and monensin had the strongest and fastest effect (Figure S2A). We were unable to detect tubules by electron microscopy of HUVECs treated with monensin for 1 hr (Figure 1D). We also tested the effect of monensin on WPBs generated in HEK293 cells after expression of the D1-A1 truncation and found that they also become round after a 1 hr treatment (Figure S2B). We conclude that VWF tubulation underpins the elongated shape of WPBs, and that both are dependent on an acidic pH. To determine the pH within WPBs, we used a functional assay, based on this change in WPB shape. Analysis of HUVECs incubated with the ionophore nigericin buffered at various pHs revealed that WPBs are predominantly round at pH 7, mostly elongated at pH 6 or pH 5.5, and exhibit an intermediate phenotype at pH 6.5 (Figure S3). This suggests that the pH within WPBs is below 6.5, but probably above pH 6 (Figure S3, legend), and confirms that an acidic pH is crucial for VWF tubulation.

VWF Tubulation Is Essential for VWF Unfurling

Upon exocytosis, VWF in WPBs is exposed to blood (pH 7.4), at which point it rapidly unfurls from the compact tubular storage format into filaments 100 times longer than the WPBs. To determine how that physiological switch in pH relates to the rounding of monensin-treated WPBs in cultured cells, we treated HUVECs with the detergent Triton X-100 (TX-100), which removed the constraining membrane from around VWF and allowed changes in the folding of VWF to be monitored by immunofluorescence microscopy. To observe intermediates of VWF unfolding, we performed this treatment on ice at various pHs dictated by our findings described above. At pH 5.6, there was very little change in VWF staining, even after 20 min of detergent treatment, such that a very compact shape, reminiscent of the rod-like WPBs, could be recognized (Figures 3A and 3B). Treatment at pH 6.4 gave an intermediate, dispersed phenotype (Figures 3C and 3D), and we were able to clearly see a VWF filament coming out of what looked like a single WPB (Figure 3D′). However, treatment at pH 7.2, mimicking the environment after exocytosis, led to a loss of

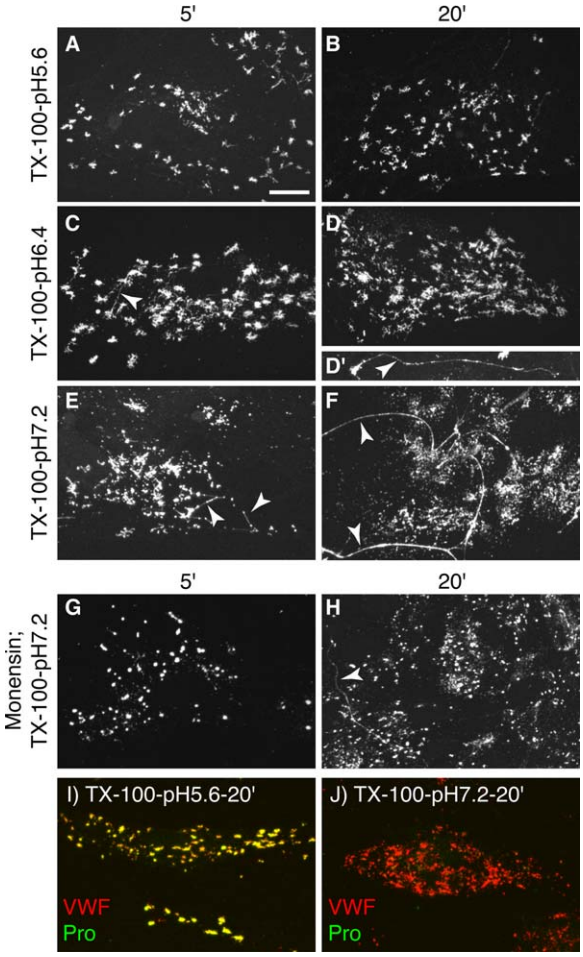

Figure 3. Storage of VWF as Tubules Promotes Its Efficient Dispersion

(A–F) HUVECs were stained for VWF during processing for immunofluorescence microscopy. Treatment with TX-100 (time is indicated above the panels) at an (A and B) acidic pH had little effect, while at a (C–D′) less acidic or at a (E and F) neutral pH it allows VWF dispersion and unfurling of long filaments (arrowheads in [C], [D′], [E], and [F]).

(G and H) Monensin treatment followed by TX-100 at a neutral pH prevents VWF dispersion, and unfurled filaments were rarely observed (arrowhead in [H]).

(I and J) HUVECs were stained for mature VWF (VWF; red) and the propeptide (Pro; green) after TX-100 treatment. Both proteins colocalize at (I) acidic pH; however, the propeptide is released at (J) neutral pH, while VWF dispersion can be observed.

In all panels, the scale bars represent 10 μm.

the distinctive rod shape, showing instead a dispersion of mature VWF (Figures 3E and 3F). Furthermore, we observed the formation of short filaments after detergent treatment of HUVECs at neutral pH after only 5 min (Figure 3E), and long filaments of 50 μm or more were common after 20 min (Figure 3F). In contrast, filaments were only very rarely seen when HUVECs were treated with detergent at acidic pH.

We hypothesized that storage of VWF as tubules avoids tangling the long VWF filaments during biogenesis: as with carefully coiled ropes, a tubular packing should allow for an easy transition from compressed to elongated VWF and could thus be a prerequisite for

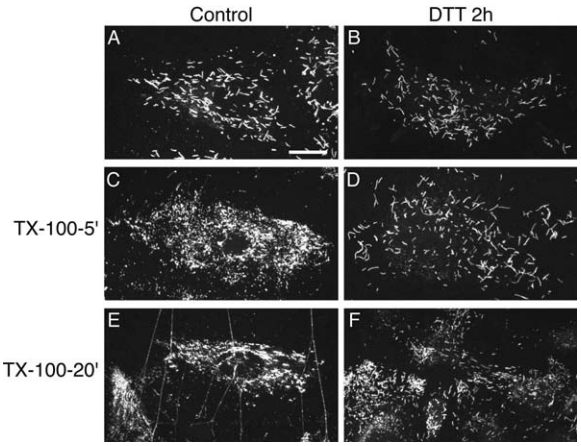

Figure 4. Maintenance of WPB Elongation Does Not Require Multimerization

(A–F) HUVECs were stained for VWF. (A) Normal WPBs are elongated. (C and E) Treatment with the detergent TX-100 at a neutral pH induces VWF dispersion. (B) DTT treatment (20 mM for 2 hr) does not affect WPB shape, and, (D and F) when followed by TX-100 at a neutral pH, it completely prevents any VWF dispersion. The scale bars represent 10 μm.

VWF dispersion and the rapid formation of long filaments at exocytosis. We therefore pretreated HUVECs with monensin for 15 min, followed by TX-100 treatment at pH 7.2. Comparing this (Figures 3G and 3H) with mock-treated cells bathed in TX-100 at pH 7.2 (Figures 3E and 3F), it was clear that both VWF dispersion and the ability to unfurl into long filaments were severely affected by treatment with monensin. We conclude that VWF tubulation is necessary for the unfolding of VWF when the membrane is removed, even in static conditions.

The propeptide is noncovalently associated with VWF multimers in WPBs (Ewenstein et al., 1987; Wagner et al., 1987), and its binding to VWF multimers is pH and calcium dependent (Vischer and Wagner, 1994). To analyze the role of the propeptide in VWF compaction, we determined its localization during detergent treatment. At pH 5.6, the propeptide exactly colocalized with compact, mature VWF, but, at pH 7.2, it was no longer associated with the dispersed VWF (Figures 3I and 3J). This implies that the compact, elongated shape of WPBs relies on a pH-dependent interaction between the propeptide and mature VWF. Together with our data from the Y87S mutant, this strongly suggests a direct role for the propeptide in VWF compaction into tubules. Increasing or decreasing the calcium concentration during detergent addition at a neutral pH did not have a significant effect on VWF dispersion (data not shown).

VWF Multimerization and Dispersion

Since the interactions within VWF leading to tubulation and to multimerization are closely related, we also tested the role of multimerization in the maintenance of WPB elongation by incubating HUVECs with 20 mM DTT for 2 hr. We could not identify any striking change in the shape of WPBs, suggesting that tubulation was not affected by the disruption of disulphide bonds (Figures 4A and 4B). Surprisingly, when these cells were

subsequently treated with PBS at pH 7.2 supplemented with 1% TX-100, we still observed no change in VWF staining (Figures 4D and 4F), to the point that these cells were indistinguishable from untreated HUVECs (Figure 4A). Although long filaments were not expected, as these are formed by multimers, we detected no dispersion at all. We conclude that the expansion of VWF is dependent on its disulphide bonds, but that tubulation itself is not affected.

Tubular Storage of VWF Is Required for the Formation of Long, Platelet-Recruiting Filaments after Exocytosis In Vitro

Our data led to the hypothesis that the tubular structure of VWF is needed to generate long VWF filaments after exocytosis. In flow chamber experiments, it has been shown that these long filaments can recruit platelets after exocytosis (Dong et al., 2002), and we used this system to further test our hypothesis. HUVECs were placed in a parallel-plate flow chamber and were perfused with culture medium and histamine (100 μM) at a constant wall shear stress of 0.25 Pa, mimicking conditions within venules (Dong et al., 2002). Histamine was perfused for 1 min, followed by histamine plus purified platelets (1×10^8/ml). Less than 1 min after platelet addition, platelets started to attach to VWF filaments (Movie S1). On average, 9.4% of stimulated HUVECs were able to generate VWF filaments that were 94 ± 11 μm long and carried 15.4 ± 1.7 platelets (Figures 5A and 5C–5E; Movie S2). We then used monensin to disassemble the VWF tubules within the WPBs of the cells before placing them in the parallel-plate flow chamber. After drug treatment, only 6.3% of the cells generated VWF filaments; furthermore, we observed a 50% decrease in the average number of platelets per filament (7.9 ± 1) and a filament length of 59 ± 6 μm (Figures 5B–5E; Movie S3). Importantly, the greatest effect is on the longest filaments (above 150 μm), which essentially disappear. Quantitation by ELISA showed that monensin does not reduce regulated secretion of VWF (Figure 5F). We also found that the number of platelets bound per micrometer of VWF filament decreased only marginally in monensin-treated cells (Figure S4). Thus, monensin does not affect VWF secretion nor its affinity for platelets, but only its ability to unfurl in long, platelet-recruiting filaments.

Monensin Treatment Impairs the Rapid Unfurling of Platelet-Recruiting VWF Filaments after Exocytosis in Mouse Venules

We next investigated the effect of monensin in vivo. In control mice, laser injury to venules induced platelet strings originating from the site of injury and extending up to 250 μm downstream within less than 10 s in general and after only 1–2 s in some instances (Figures 6A, 6B, and 6E; Movie S4). Mice pretreated with monensin before surgery (100 μM, 200 μl intrascrotal for 1 hr) generated strings that were three times shorter than those in control mice (Figures 6C and 6E). Strings were transient in nature and usually disappeared from venules within 30 s of injury (Figure 6F), which is consistent with a previous in vitro report (Dong et al., 2002). In both control and monensin-treated vessels, platelets appeared to translocate along the string in the direction of flow rather than being stably adherent.

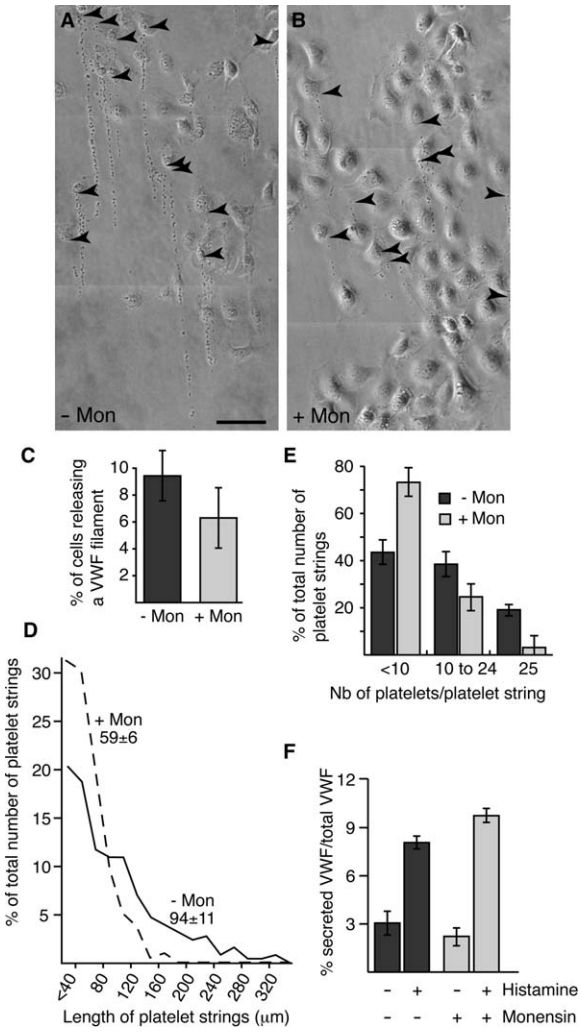

Figure 5. Disassembly of VWF Tubules Reduces the Length of Platelet-Recruiting Filaments from HUVECs Stimulated under Flow

(A and B) Untreated (− Mon) or monensin-treated (+ Mon) HUVECs were incorporated into a parallel plate flow chamber. Histamine, followed 1 min later by histamine plus platelets, was perfused across the HUVECs at a wall shear stress of 0.25 Pa for 10 min, during which formation of platelet strings was recorded. Three consecutive fields were captured to create the pictures. Arrowheads point to the origin of individual platelet strings. "Levels" were adjusted in Photoshop to enhance platelet string visibility (arrowheads). The scale bar represents 50 μm.

(C) A total of 50 fields were analyzed for the number of cells releasing at least 1 filament. Bars indicate the percentage ± standard deviation (n = 4 experiments).

(D and E) All observable individual strings of platelets were analyzed for (D) length and (E) number of attached platelets. Numbers in (D) and bars in (E) indicate the mean ± standard deviation (n = 4 experiments).

(F) A VWF-ELISA was performed after a 10 min stimulation or mock stimulation with histamine of untreated or monensin-treated cells.

In separate experiments, we increased exposure to monensin by superfusing it directly onto the cremaster muscle for 30 min (100 μM, 8 ml/min) prior to laser injury. In these experiments, we routinely observed tangled platelet strings (Figure 6D; Movie S5), which resembled balls that were distinct from thrombi, required only weak laser injury, and formed almost immediately.

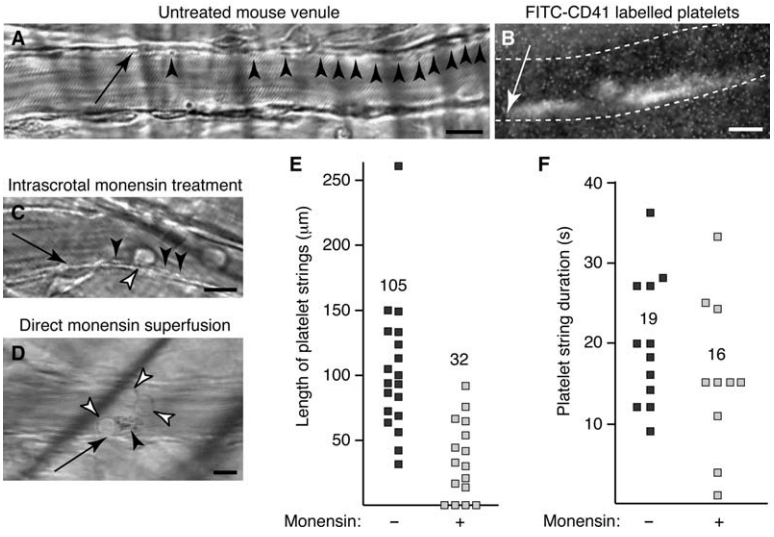

Figure 6. Monensin Treatment Disrupts the Formation of Injury-Induced Platelet Strings in Mice Venules

(A–D) (A and B) Control or (C and D) monensin-treated mouse cremasters were observed for platelet string formation after laser injury. Flow is from left to right. Arrows point to the position of laser injury; black arrowheads point to individual platelets or groups of platelets along the string; white arrowheads indicate rolling leukocytes. "Levels" were adjusted in Photoshop to enhance platelet visibility. (A and B) Laser-induced platelet interactions in a postcapillary venule of a control mouse. (A) Platelets are visible as black punctae. (B) FITC-CD41-labeled platelets were infused to confirm the identity of the black punctae. The image is a maximum intensity projection of 100 slices of a stack collected at 3 slices per second. Dotted lines indicate the approximate locations of vessel walls. (C and D) Laser-induced platelet interaction in a mouse treated with monensin by (C) instrascrotal pretreatment (three platelets are visible as white punctae in a row) or (D) direct superfusion (super-stable tangled knot of platelets). In all panels, scale bars represent 10 μm.

(E and F) (E) Length and (F) stability of individual platelet strings were determined in 10–19 venules from 5 untreated and 4 monensin-pretreated (instrascrotal) mice. This does not take into account the data involving tangled platelet balls from direct superfusion. The numbers indicate the mean.

Approximately 50% of these tangles washed immediately downstream; however, those remaining attached were still present after 1 hr.

The observation of leukocytes rolling on the endothelial surface in monensin-treated mice (Figures 6C and 6D; see also Movie S5, in which three leukocytes can be observed starting to roll only after the laser-induced injury) provided an internal control for WPB exocytosis in these experiments; this rolling reflects the appearance of the leukocyte receptor P-selectin (Moore et al., 1995).

Discussion

Rod-shaped WPBs are a classic hallmark of endothelial cells. We find that the elongated shape of WPBs depends on the ability of VWF to form tubules. We also show that both the propeptide and the N-terminal D′-A1 domains of mature VWF are necessary and sufficient for tubule formation. The maintenance of tubules, and thus WPB shape, is also dependent on the low pH that is essential for the propeptide to bind mature VWF. We find that the rapid unfurling, after exocytosis, of the long filaments that permit initial recruitment of platelets at sites of endothelial cell injury correlates with the storage of VWF in tubules. Thus, the shape of this organelle is essential to its cargo's function because the hemostatic function of VWF depends on its storage in tubules. The storage format of a cargo can therefore directly influence the function of that cargo after exocytosis.

Whether the fraction of platelet binding dependent on tubular storage of VWF is needed to avoid bleeding is currently unclear. For example, chloroquine, widely used for prevention and treatment of malaria and (as an anti-inflammatory agent) several auto-immune diseases, has the side effect of causing bleeding. Based on the data presented here, we speculate that this reflects the predicted decreased ability to recruit platelets to VWF. However, chloroquine also has direct effects on platelets, precluding a simple interpretation.

pH and the Maintenance of Tubulation

The importance of pH to VWF tubulation was revealed by using four different treatments to neutralize the intra-WPB environment. After monensin treatment, WPBs lack the internal striations that represent VWF tubules in longitudinal section, and this effect is not reversible (Lui-Roberts et al., 2005). Monensin and other pH-altering drugs have been shown in the past to interfere with VWF multimerization and glycosylation (Vischer and Wagner, 1994; Wagner et al., 1985, 1986), but the incubation times used were very long (several days), and the effects were likely due to the consequences of neutralization of pH within the Golgi apparatus and the TGN, blocking the formation of new multimers. We used short incubation times to examine the effect of monensin on preexisting WPBs (we estimate that 95% of WPBs affected by monensin were formed before the treatment) that will not affect VWF multimerization, since this is dependent on the formation of disulphide bonds in the ER and the Golgi. Further, if neutralizing the pH in WPBs were to disassemble multimers, then only monomers would be seen in plasma. In fact, proteolysis by ADAMTS13 is required to reduce the size of VWF multimers to those seen in blood (Dong et al., 2002).

Our results show that an acidic pH is required for stabilization of VWF tubules, and that the shape of WPBs is closely related to the tubular conformation of VWF. Consistent with these results, removal of the limiting membranes by treatment with detergent results in VWF dispersion at a neutral pH, but retention of a very compact shape when an acidic medium is used with the detergent. These results correlate with our finding that the pH within WPBs is likely to be between 6 and 6.5. We conclude that VWF tubulation, dependent on noncovalent interactions, underpins WPB elongation.

Formation of VWF Tubules

To determine which domains of VWF are important for elongation, we used heterologous expression of VWF in HEK293 cells (Michaux et al., 2003). We could not detect elongated WPBs after expression of either the propeptide or mature VWF, indicating that domains in both peptides are required for tubulation. We also found that expression of a truncated protein comprising the propeptide and the D′-A1 domains of mature VWF is sufficient to allow formation and storage of monensin-sensitive tubules in elongated WPBs. Since the truncated protein cannot multimerize, this indicates that an intact propeptide and the D′-A1 domains are sufficient for VWF tubulation, independent of multimerization. This surprising result—that tubulation and multimerization are independent—is confirmed by our data from DTT treatment.

Among the mutations we have expressed in HEK293 cells, only Y87S affects WPB elongation and thus tubulation; but, as it also completely blocks multimerization, we have not been able to separate these two processes on the basis of human disease-causing mutations. Indeed, we would now argue that mutations affecting the propeptide or the D′-A1 domains of mature VWF might not only directly affect platelet binding, but also tubulation, thereby indirectly interfering with VWF function in platelet recruitment.

VWF Storage Format and Function

Because we have shown that monensin does not significantly affect VWF secretion, affinity for platelets, or filament stability—as long as it is not a tangle—we conclude that its only effect is to disrupt the tubular conformation of VWF inside WPBs. The simplest explanation for VWF storage in tubules is that it prevents entanglement of the multimer and allows for its rapid unfurling. If, instead, it is kept in a disorganized storage format, as after monensin treatment, then, upon exocytosis, the VWF multimer cannot unfurl properly, but rather generates a short or tangled filament. From the flow cell experiments, by combining the percentage of cells able to generate a filament with the average number of platelets carried by these filaments, we find that 100 HUVECs will capture 145 platelets (i.e., multiplying 9.4 cells generating filaments by the average 15.4 platelets captured by a given filament), compared to only 50 platelets for 100 monensin-treated HUVECs—a 65% decrease in VWF efficiency. That some VWF filaments can undergo partial extension after monensin treatment probably reflects that some unfolding, possibly aided by flow, can occur when tangles and knots have been randomly avoided. While this leads to an apparent mismatch between the dramatic effects of monensin on shape and the more partial effect on filament length, these simple quantitative analyses may underestimate the effects of treatment, since monensin has its greatest effect on the longest strings, which are thought to be disproportionately important to VWF function.

The surprising stability of the monensin-induced VWF tangles indicates that they are resistant to the metalloprotease ADAMTS13; presumably, an orderly string under flow facilitates exposure of the cleavage site to the protease. ADAMTS13 cleaves the long VWF multimers within 30–60 s (Dong et al., 2002) to prevent anarchic clotting and platelet depletion, leading to bleeding. Indeed, mutations in ADAMTS13 are responsible for the rare bleeding disorder thrombotic thrombocytopenic purpura (Levy et al., 2001). The dangerous ultrathrombogenic potential of the long VWF filaments is therefore normally strictly limited to the site of injury. But, it makes it even more crucial to unfurl as long a filament as possible very rapidly so as to recruit the maximum number of platelets in the minimum time. We therefore hypothesize that VWF mutations affecting tubulation could induce thrombotic thrombocytopenic purpura in an ADAMTS13 wild-type context as well as von Willebrand's disease.

VWF Tubules Might Be Constrained Springs

Cargo condensation is central to secretory granule biogenesis, but we now argue that it can be more than simply a device to maximize storage; it can also be essential to a cargo's physiological function after exocytosis. VWF unfurling is a very rapid process: in laser-injured mice, we observed some platelet strings or tangles only 1–2 s after the first hit, faster than the 15 s delay reported after stimulation with the calcium ionophore A23187 (Andre et al., 2000). During this time, events that may include signal transduction, docking of WPBs, fusion of the membranes, unfurling of the VWF filament, and recruitment of platelets, must all occur, which leaves a very short time for a 100-fold expansion of the VWF multimer. It is possible that the filament is pulled out by fluid flowing past the fusion pore, rather than pushed out by VWF unfolding driven by the pH switch. However, we would argue that the appearance of filaments in our static immunofluorescence experiments, even when done on ice, strongly argues that even if it makes a contribution, flow cannot provide a full explanation for filament extension.

The structure of VWF in the tubules is not known, except that they appear in electron microscopy to form hollow cylinders (Figure S1B) and that they are rigid (data not shown). Furthermore, in solution, VWF multimers can adopt a random coiled conformation (Fowler et al., 1985; Slayter et al., 1985). Under flow, the filaments stretch or contract as flow is increased or decreased (Dong et al., 2002; our unpublished data). On the bases of these data, we propose a speculative model: we hypothesize that the tubules are VWF multimers coiled into a constrained spring at low pH, and that the propeptide is at least partly responsible for this constraint.

The propeptide, which is rapidly lost after secretion (Hannah et al., 2005) and has no known physiological function in the blood, was thought only to be required as an oxidoreductase during multimerization (Purvis and Sadler, 2004; Vischer and Wagner, 1994) and for storage of mature VWF (Haberichter et al., 2000, 2003). We now show that the interaction between the propeptide and mature VWF in WPBs correlates with their elongated shape and the release of the filaments when the pH is raised. This is consistent with a previous report showing that the propeptide is released from binding to mature VWF upon exocytosis at neutral, but not acidic, pH (Vischer and Wagner, 1994). We therefore propose that a pH-dependent interaction of the propeptide with VWF in WPBs is required to constrain VWF into a spring-like structure, and that, upon exocytosis, propeptide dissociation allows filament unfurling (Figure 7).

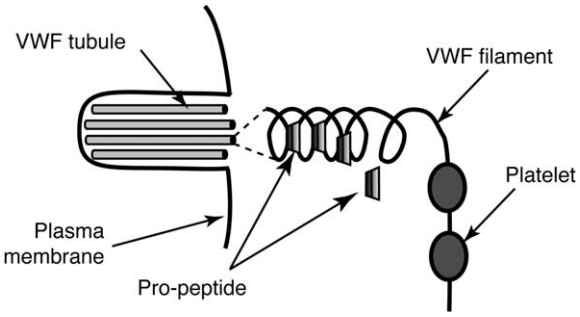

Figure 7. A Speculative Model of VWF Unfurling from Tubules to Long Platelet-Recruiting Filaments

Upon exocytosis of a WPB (left, with VWF tubules), the propeptide falls off as the pH rises, and the VWF multimer unfurls in a long filament to recruit platelets.

The dissociation of the propeptide upon exocytosis might therefore be a necessity rather than a default fate. The most likely explanation of the monensin effect is that of a detachment of the propeptide leading to a premature unfurling of the VWF filament inside WPBs.

Structural studies of the tubules are also essential to better understand how VWF unfurling might be affected by VWF mutations and cause bleeding in an unexpected manner. We also show here that at least one drug used to treat several diseases has an effect on VWF tubules, and this could be true of any other drug altering intraorganellar pH, potentially explaining bleeding side effects, but also perhaps providing a new way of controlling VWF physiological function in hemostasis without affecting the inflammatory function of P-selectin.

Experimental Procedures

Cell Culture, Transfection, and Reagents

Human umbilical vein endothelial cells (HUVEC) were purchased from Cascade Biologicals (Portland, OR). The cells were grown in M199 (GIBCO-BRL, Grand Island, NY) with 20% fetal calf serum (Hyclone, Logan, UT), 10 U/ml heparin (Sigma, St. Louis, MO), 50 μg/ml gentamicin, and 30 μg/ml endothelial cell growth supplement (Sigma). HEK293 cells were provided by BD Biosciences (Oxon, United Kingdom) and were grown in α-minimum essential medium (α-MEM) (Life Technologies, Paisley, United Kingdom), 10% fetal calf serum, and 50 μg/ml gentamicin (Life Technologies). Cells were transiently transfected by Nucleofection (Amaxa, Cologne, Germany) according to the manufacturer's instructions.

Monensin (Sigma) was used at a 10 μM final concentration for 1 hr unless stated otherwise and was diluted in growth medium, saline, or in superfusion buffer. NH_4Cl, nigericin, and chloroquine (Sigma) were used, respectively, at 20 mM, 10 μM, and 100 μM final concentration in growth medium. Triton X-100 (Sigma) was used at 1% in PBS after pH adjustment. The detergent was applied on ice for 20 min. DTT (Sigma) was used at 20 mM for 2 hr.

Expression Vectors

VWF constructs Pro and Δpro have been described (Haberichter et al., 2000), as has the Y87S VWF variant (Rosenberg et al., 2002). The D1-D3 construct was obtained by PCR and subcloning with the template pVW198.1 (Kroner et al., 1991). A 1302 base pair PCR product was generated with the primer s-VWF-2373 (5′-GTGCCAG AACTATGACCTGGAGTGCATGAGCATGGGCTGT-3′) and a mutagenic anti-sense primer, a-VWF-"3675" (5′-atctagaattcg^{3663}GTGCT CAGGGTCACTGG-3′), containing an stop codon and an engineered EcoRI site for cloning. The capitalized sequence is the normal VWF sequence. The 985 base pair BamHI/EcoRI-digested PCR product was ligated to the 2800 base pair AvrII/BamHI fragment of pVW198.1 and the 4695 base pair NheI/EcoRI fragment of pEGFP-N1 to create pEGFP-D3, taking advantage of the NheI/AvrII compatible cohesive ends. A similar strategy was used to create two additional vectors, pCMV-VWF-D3-c-*myc*, which contains a c-*myc* tag rather than GFP, and pCIneo-VWF-D3, which does not contain a c-*myc* epitope or GFP tag. The D1-A1 construct was obtained by using the full-length VWF expression vector, pCIneo-VWF-ES (previously described), as a template: an 851 base pair PCR product was generated with primer s-VWF-3598 (5′-GAGaTGcaTGGCCGG CGTTTTGCCTCAGGA-3′) and a-VWF 4449 min (5′-CAAGAGCggC cGctaCACAGTGACTTGTGC-3′) to introduce a stop codon, followed by a NotI restriction site at the 3′ end of the construct. Normal VWF sequence is indicated by uppercase letters. The resulting PCR product was cloned into the Bsu36I/NotI site of the shuttle vector, pG11vW1, that contains the BamHI/NotI fragment of pCIneo-VWF-ES cloned into the pGEM-11 cloning vector (Promega). PG11vW1 was then digested with BamHI and NotI, and the resulting 1721 base pair fragment was ligated to the 2360 base pair XbaI/BamHI and the 5806 base pair XbaI/NotI fragments of pCIneo-VWF-ES to create pCIneo-VWF-A1.

GFP, Antibodies, and Microscopy

Sheep polyclonal anti-human VWF was purchased from Serotec (Oxford, United Kingdom). The monoclonal anti-VWF-propeptide 239.1 has been described (Haberichter et al., 2000). Secondary antibodies coupled to fluorophores were purchased from Jackson (Luton, United Kingdom). FITC-labeled anti-mouse CD41 was purchased from BD-Pharmingen (Oxford, United Kingdom). For immunofluorescence studies, antibody staining and confocal microscopy were carried out as previously described (Blagoveshchenskaya et al., 2002). In Figure 1B, data were collected 48 hr after nucleofection and are projections of confocal sections throughout the cells.

While the figures of this paper generally show very few cells, great care was taken to ensure that these are representative of the data. Indeed, the drugs and detergent that were used had a very homogenous and reproducible effect.

Electron Microscopy

HUVECs were plated onto 10 or 13 mm diameter coverslips for embedding en face. Cells were fixed in 2% paraformaldehyde/1.5% glutaraldehyde in M199/20 mM HEPES. After monensin treatment, cells were fixed with 2% paraformaldehyde/1.5% glutaraldehyde in 0.1 M sodium cacodylate buffer or in M199/20 mM HEPES for 20 min at room temperature. The cells were then postfixed in 1% osmium tetroxide/1.5% potassium ferricyanide and treated with tannic acid as described previously (Simionescu and Simionescu, 1976). The samples were then embedded in epon by conventional procedures. Coverslips were removed by plunging the samples into liquid nitrogen, leaving the cells embedded on the epon. Sections (60 nm) were then cut with a Leica Ultracut UCT microtome (Leica, Vienna, Austria), stained with lead citrate, and viewed with a transmission electron microscope (EM420; Philips, Eindhoven, the Netherlands).

Platelet Preparation

Venous blood was collected from healthy human adult volunteers into acid-citrate-dextrose (ACD) anticoagulant. Blood was centrifuged at 200 × g for 10 min to produce platelet-rich plasma (PRP). PRP was collected and reacidified by the addition of ACD before the platelets were pelleted by centrifugation at 300 × g for 20 min. Plasma was removed, and platelets were resuspended at 1 × 10^8/ml in HEPES Tyrode buffer.

In Vitro Platelet String Formation

HUVECs were plated onto 35 mm Petri dishes and treated with 10 μM monensin or control for 1 hr. The Petri dishes were then incorporated into a parallel-plate chamber (Glycotech, MD, USA) and connected to a syringe pump that drew fluid through the chamber at a flow rate giving a wall shear stress of 0.25 Pa (2.5 dyn/cm^2). The inlet of the flow chamber was connected to an electronic valve allowing switching between perfusions of histamine (Sigma; 100 μM in HUVEC growth medium without plasma) or platelets and histamine. The chamber was mounted on a phase-contrast video-microscope (Nikon Eclipse TE300), enclosed at 37°C.

Histamine diluted in HUVEC culture medium without serum was perfused across HUVECs for 11 min to stimulate VWF release; perfusion of platelets started 1 min after the histamine stimulation began. During this 10 min period, a series of fields were scanned and recorded for later off-line analysis. Platelet strings could be visualized directly and were also video recorded with a 1/2″ 3-CCD camera (Hitachi HV-C20A, Hitachi Denshi, Leeds, UK) onto mini-DV cassettes. Video recordings were transferred to an Apple computer and then analyzed with iMovie (Apple). Still pictures were then extracted and analyzed with Openlab (Improvision) to determine the length of each individual platelet string (as defined by the cell from which the filament originated to the last platelet attached to it) and the number of platelets attached.

In Vivo Platelet String Formation

Male C57BL/6 mice (20–30 g) were purchased from Harlan. All procedures were approved by the University of Sheffield ethics committee and performed in accordance with Home Office Animals (Scientific Procedures) Act 1986. Mice were anaesthetized and prepared for intravital microscopy of the cremaster muscle as described (Norman et al., 2000). Mice were either pretreated with intrascrotal monensin (200 μl; 100 μM in saline) prior to surgery or received a continuous superfusion of 100 μM monensin directly onto the prepared cremaster muscle for 30 min before microscopy began. During intravital microscopy recording, the cremaster muscle was superfused with thermocontrolled (36°C) bicarbonate-buffered salt solution.

Cremaster venules and arterioles (20–50 μm) were observed with a light microscope (Nikon Eclipse E600-FN, Nikon UK Ltd) equipped with a water immersion objective (40×/0.80 W). Endothelial injury was induced in up to ten microvessels (venules and arterioles) per animal by using a pulsed nitrogen dye laser (Photonic Instruments, St. Charles, IL) applied through the microscope objective. Laser energy was attenuated to a lower level than typically required for thrombus generation by using a variable neutral density filter, and the laser was fired at a frequency of approximately 1 Hz until evidence of string formation was detected (usually within 5 s). Images were captured with a three chip 1/3″ CCD camera (Dage MTI DC-330, DAGE MTI, Inc., Michigan City, IN) and were recorded onto mini-DV cassettes for later off-line analysis. Some mice received 5 μg anti-CD41 antibody to preferentially label platelets as described (Falati et al., 2002). In these experiments, vessels were imaged in brightfield and under fluorescence by using an automated excitation filter changer (Lamba DG4, Sutter Novato, CA), an intensified (GenIII, Videoscope, Dulles, VA) camera system (Sensicam, Cooke, Auburn Hills, MI), and Slidebook software (Intelligent Imaging Innovations, Denver, CO).

Sequences were captured onto an Apple G5 computer by using Final Cut Pro software (Apple Computers Inc.) and were analyzed with the public domain NIH-Image program (available on the internet at http://rsb.info.nih.gov/nih-image). Platelet string length was measured from the point of endothelial injury to the farthest point of platelet adhesion. String duration was determined as the time between initiation and termination of visible platelet interaction. Vessel diameter, center-line velocity, and shear rate were determined as described (Norman, 2001).

Supplemental Data

Supplemental Data including four figures and five movies are available at http://www.developmentalcell.com/cgi/content/full/10/2/223/DC1/.

Acknowledgments

We thank Alan Hall, Martin Raff, and members of the Cutler lab for critical reading of the manuscript. We thank Mark Marsh for helpful discussions. Work in D.F.C.'s lab is supported by the Medical Research Council of Great Britain. G.M. was supported by a Marie Curie fellowship of the European Union. The K.E.N. lab is supported by a Career Establishment Grant from the Medical Research Council of Great Britain. The Haberichter lab is supported by the American Heart Association (SDG 0435466N), a Hemophilia Association of New York Research Grant, and the Children's Hospital Research Foundation.

Received: April 13, 2005
Revised: October 25, 2005
Accepted: December 8, 2005
Published: February 6, 2006

References

Andre, P., Denis, C.V., Ware, J., Saffaripour, S., Hynes, R.O., Ruggeri, Z.M., and Wagner, D.D. (2000). Platelets adhere to and translocate on von Willebrand factor presented by endothelium in stimulated veins. Blood *96*, 3322–3328.

Blagoveshchenskaya, A.D., Hannah, M.J., Allen, S., and Cutler, D.F. (2002). Selective and signal-dependent recruitment of membrane proteins to secretory granules formed by heterologously expressed von Willebrand factor. Mol. Biol. Cell *13*, 1582–1593.

Dong, J.F., Moake, J.L., Nolasco, L., Bernardo, A., Arceneaux, W., Shrimpton, C.N., Schade, A.J., McIntire, L.V., Fujikawa, K., and Lopez, J.A. (2002). ADAMTS-13 rapidly cleaves newly secreted ultralarge von Willebrand factor multimers on the endothelial surface under flowing conditions. Blood *100*, 4033–4039.

Ewenstein, B.M., Warhol, M.J., Handin, R.I., and Pober, J.S. (1987). Composition of the von Willebrand factor storage organelle (Weibel-Palade body) isolated from cultured human umbilical vein endothelial cells. J. Cell Biol. *104*, 1423–1433.

Falati, S., Gross, P., Merrill-Skoloff, G., Furie, B.C., and Furie, B. (2002). Real-time in vivo imaging of platelets, tissue factor and fibrin during arterial thrombus formation in the mouse. Nat. Med. *8*, 1175–1181.

Fowler, W.E., Fretto, L.J., Hamilton, K.K., Erickson, H.P., and McKee, P.A. (1985). Substructure of human von Willebrand factor. J. Clin. Invest. *76*, 1491–1500.

Haberichter, S.L., Fahs, S.A., and Montgomery, R.R. (2000). von Willebrand factor storage and multimerization: 2 independent intracellular processes. Blood *96*, 1808–1815.

Haberichter, S.L., Jacobi, P., and Montgomery, R.R. (2003). Critical independent regions in the VWF propeptide and mature VWF that enable normal VWF storage. Blood *101*, 1384–1391.

Hannah, M.J., Skehel, P., Erent, M., Knipe, L., Ogden, D., and Carter, T. (2005). Differential kinetics of cell surface loss of von Willebrand factor and its propolypeptide after secretion from Weibel-Palade bodies in living human endothelial cells. J. Biol. Chem. *280*, 22827–22830.

Kroner, P.A., Friedman, K.D., Fahs, S.A., Scott, J.P., and Montgomery, R.R. (1991). Abnormal binding of factor VIII is linked with the substitution of glutamine for arginine 91 in von Willebrand factor in a variant form of von Willebrand disease. J. Biol. Chem. *266*, 19146–19149.

Levy, G.G., Nichols, W.C., Lian, E.C., Foroud, T., McClintick, J.N., McGee, B.M., Yang, A.Y., Siemieniak, D.R., Stark, K.R., Gruppo, R., et al. (2001). Mutations in a member of the ADAMTS gene family cause thrombotic thrombocytopenic purpura. Nature *413*, 488–494.

Lui-Roberts, W.W., Collinson, L.M., Hewlett, L.J., Michaux, G., and Cutler, D.F. (2005). An AP-1/clathrin coat plays a novel and essential role in forming the Weibel-Palade bodies of endothelial cells. J. Cell Biol. *170*, 627–636.

Michaux, G., and Cutler, D.F. (2004). How to roll an endothelial cigar: the biogenesis of Weibel-Palade bodies. Traffic *5*, 69–78.

Michaux, G., Hewlett, L.J., Messenger, S.L., Goodeve, A.C., Peake, I.R., Daly, M.E., and Cutler, D.F. (2003). Analysis of intracellular storage and regulated secretion of 3 von Willebrand disease-causing variants of von Willebrand factor. Blood *102*, 2452–2458.

Moore, K.L., Patel, K.D., Bruehl, R.E., Li, F., Johnson, D.A., Lichenstein, H.S., Cummings, R.D., Bainton, D.F., and McEver, R.P. (1995). P-selectin glycoprotein ligand-1 mediates rolling of human neutrophils on P-selectin. J. Cell Biol. *128*, 661–671.

Norman, K.E. (2001). An effective and economical solution for digitizing and analyzing video recordings of the microcirculation. Microcirculation *8*, 243–249.

Norman, K.E., Katopodis, A.G., Thoma, G., Kolbinger, F., Hicks, A.E., Cotter, M.J., Pockley, A.G., and Hellewell, P.G. (2000). P-selectin

glycoprotein ligand-1 supports rolling on E- and P-selectin in vivo. Blood *96*, 3585–3591.

Purvis, A.R., and Sadler, J.E. (2004). A covalent oxidoreductase intermediate in propeptide-dependent von Willebrand factor multimerization. J. Biol. Chem. *279*, 49982–49988.

Rosenberg, J.B., Haberichter, S.L., Jozwiak, M.A., Vokac, E.A., Kroner, P.A., Fahs, S.A., Kawai, Y., and Montgomery, R.R. (2002). The role of the D1 domain of the von Willebrand factor propeptide in multimerization of VWF. Blood *100*, 1699–1706.

Ruggeri, Z.M. (2003a). Von Willebrand factor. Curr. Opin. Hematol. *10*, 142–149.

Ruggeri, Z.M. (2003b). Von Willebrand factor, platelets and endothelial cell interactions. J. Thromb. Haemost. *1*, 1335–1342.

Sadler, J.E. (1998). Biochemistry and genetics of von Willebrand factor. Annu. Rev. Biochem. *67*, 395–424.

Sadler, J.E. (2005). New concepts in von Willebrand disease. Annu. Rev. Med. *56*, 173–191.

Simionescu, N., and Simionescu, M. (1976). Galloylglucoses of low molecular weight as mordant in electron microscopy. I. Procedure, and evidence for mordanting effect. J. Cell Biol. *70*, 608–621.

Slayter, H., Loscalzo, J., Bockenstedt, P., and Handin, R.I. (1985). Native conformation of human von Willebrand protein. Analysis by electron microscopy and quasi-elastic light scattering. J. Biol. Chem. *260*, 8559–8563.

van Mourik, J.A., Romani de Wit, T., and Voorberg, J. (2002). Biogenesis and exocytosis of Weibel-Palade bodies. Histochem. Cell Biol. *117*, 113–122.

Vischer, U.M., and Wagner, D.D. (1994). von Willebrand factor proteolytic processing and multimerization precede the formation of Weibel-Palade bodies. Blood *83*, 3536–3544.

Wagner, D.D., Olmsted, J.B., and Marder, V.J. (1982). Immunolocalization of von Willebrand protein in Weibel-Palade bodies of human endothelial cells. J. Cell Biol. *95*, 355–360.

Wagner, D.D., Mayadas, T., Urban-Pickering, M., Lewis, B.H., and Marder, V.J. (1985). Inhibition of disulfide bonding of von Willebrand protein by monensin results in small, functionally defective multimers. J. Cell Biol. *101*, 112–120.

Wagner, D.D., Mayadas, T., and Marder, V.J. (1986). Initial glycosylation and acidic pH in the Golgi apparatus are required for multimerization of von Willebrand factor. J. Cell Biol. *102*, 1320–1324.

Wagner, D.D., Fay, P.J., Sporn, L.A., Sinha, S., Lawrence, S.O., and Marder, V.J. (1987). Divergent fates of von Willebrand factor and its propolypeptide (von Willebrand antigen II) after secretion from endothelial cells. Proc. Natl. Acad. Sci. USA *84*, 1955–1959.

Wagner, D.D., Saffaripour, S., Bonfanti, R., Sadler, J.E., Cramer, E.M., Chapman, B., and Mayadas, T.N. (1991). Induction of specific storage organelles by von Willebrand factor propolypeptide. Cell *64*, 403–413.

Weibel, E.R., and Palade, G.E. (1964). New cytoplasmic components in arterial endothelia. J. Cell Biol. *23*, 101–112.

Wise, R.J., Barr, P.J., Wong, P.A., Kiefer, M.C., Brake, A.J., and Kaufman, R.J. (1990). Expression of a human proprotein processing enzyme: correct cleavage of the von Willebrand factor precursor at a paired basic amino acid site. Proc. Natl. Acad. Sci. USA *87*, 9378–9382.